AGU PUBLICATIONS

Water Resources Research

RESEARCH ARTICLE
10.1002/2016WR020333

Key Points:
- Pollutant degradation during MAR has been tested under chaotic flow
- Chaotic flow enhances the spreading of recharged water in MAR
- Mixing of recharge and indigenous water promotes different redox states

Supporting Information:
- Supporting Information S1
- Movie S1

Correspondence to:
P. Rodríguez-Escales,
paula.rodriguez.escales@upc.edu

Citation:
Rodríguez-Escales, P., D. Fernàndez-Garcia, J. Drechsel, A. Folch, and X. Sanchez-Vila (2017), Improving degradation of emerging organic compounds by applying chaotic advection in Managed Aquifer Recharge in randomly heterogeneous porous media, *Water Resour. Res.*, *53*, 4376–4392, doi:10.1002/2016WR020333.

Received 27 DEC 2016
Accepted 8 MAY 2017
Accepted article online 12 MAY 2017
Published online 31 MAY 2017

Improving degradation of emerging organic compounds by applying chaotic advection in Managed Aquifer Recharge in randomly heterogeneous porous media

P. Rodríguez-Escales[1,2], D. Fernàndez-Garcia[1,2], J. Drechsel[3], A. Folch[1,2], and X. Sanchez-Vila[1,2]

[1]Department of Civil and Environmental Engineering, Universitat Politècnica de Catalunya, Barcelona, Spain, [2]Associated Unit, Hydrogeology Group (UPC-CSIC), Barcelona, Spain, [3]Institute for Applied Geosciences, Technical University Darmstadt, Darmstadt, Germany

Abstract Improving degradation rates of emerging organic compounds (EOCs) in groundwater is still a challenge. Although their degradation is not fully understood, it has been observed that some substances are preferably degraded under specific redox conditions. The coupling of Managed Aquifer Recharge with soil aquifer remediation treatment, by placing a reactive layer containing organic matter at the bottom of the infiltration pond, is a promising technology to improve the rate of degradation of EOCs. Its success is based on assuming that recharged water and groundwater get well mixed, which is not always true. It has been demonstrated that mixing can be enhanced by inducing chaotic advection through extraction-injection-engineering. In this work, we analyze how chaotic advection might enhance the spreading of redox conditions with the final aim of improving degradation of a mix of benzotriazoles: benzotriazole, 5-methyl-benzotriazole, and 5-chloro-benzotriazole. The degradation of the first two compounds was fastest under aerobic conditions whereas the third compound was best degraded under denitrification conditions. We developed a reactive transport model that describes how a recharged water rich in organic matter mixes with groundwater, how this organic matter is oxidized by different electron acceptors, and how the benzotriazoles are degraded attending for the redox state. The model was tested in different scenarios of recharge, both in homogenous and in heterogenous media. It was found that chaotic flow increases the spreading of the plume of recharged water. Consequently, different redox conditions coexist at a given time, facilitating the degradation of EOCs.

1. Introduction

Managed aquifer recharge (MAR) is a well-established technology to transfer water from surface to the underlying aquifer. Nowadays, MAR is applied worldwide. An example is the Mediterranean basin, a densely populated area heavily impacted by human activities (urban, industrial, and agricultural). Improving water security in this region is crucial to guarantee the area's future socioeconomic development. Furthermore, the availability of water resources is in risk due to climate change and population increasing [*Giorgi and Lionello*, 2008; *IPCC*, 2007; *Pedretti et al*., 2012].

MAR technology is preventing loss of large volumes of water to the sea in the form of discharge from rivers or directly as treated or untreated wastewater. The two most common sources of water in MAR systems are surface water and effluents of waste water treatment plants, in both cases containing substances in concentrations above drinking water standards. Besides traditional pollutants, emerging organic compounds (EOCs) have raised a new social concern. These compounds are associated with chemicals used in urban environments (pharmaceuticals, personal care, or life style products), industrial areas (additives, surfactants, flame retardants), and agricultural zones (pesticides, antibiotics used in veterinary activities). EOCs have been detected in all types of water bodies, from surface [*Banjac et al*., 2015; *Navarro-Ortega et al*., 2012] to subsurface [*Jurado et al*., 2012; *López-Serna et al*., 2013].

MAR technologies need not only to promote the storage of available water in aquifers, but also to improve the recharged water quality in terms of reduction in the concentrations of macro and micropollutants. Thus, merging MAR with a soil-aquifer remediation treatment (SAT) could be a smart solution. A successful experience in this regard is the installation of a permeable reactive layer at the bottom of an infiltration pond in

the Llobregat basin MAR facility located near Barcelona, Spain [*Valhondo et al*., 2014, 2015]. In this MAR-SAT system, the reactive layer is the source of labile organic carbon, which ultimately favors the occurrence of redox processes which enhance the degradation of both macro and micropollutants. However, results showed that the poor mixing between the recharged water (rich in organic matter) and the indigenous groundwater (poor in organic matter) hindered the occurrence of reactions and the subsequent degradation of pollutants [*Valhondo et al*., 2014].

In general, most in situ remediation schemes require the injected solution to mix with the indigenous groundwater. Yet, accomplishing full mixing in aquifers is challenging since the laminar flows characteristic of porous media preclude the development of turbulent eddies that typically promote mixing in open channels or engineered reactors. Actually, mixing is driven mainly by transverse dispersion processes [*Cirpka et al*., 1999; *Rolle et al*., 2009], which is a relatively slow process, and thus often insufficient to ensure the degradation of pollutants. For this reason, in the last years, several authors have been investigating how mixing can be enhanced externally through the application of pumping sequences around the target solution [*Lester et al*., 2010; *Piscopo et al*., 2013; *Trefry et al*., 2012; *Zhang et al*., 2009]. These authors numerically demonstrated that a sequence of injections and extractions from wells can generate chaotic advection in aquifers, resulting from transient velocity fields characterized by highly complicated particle trajectories [*Bagtzoglou and Oates*, 2007], for instance, forcing streamlines from pumping well pairs to superimpose [*Smale*, 1993]. By repeating flow sequences, the fluid is stretched and folded, enhancing mixing [*Trefry et al*., 2012].

There are different injection/extraction strategies proposed in the literature to maximize the effect of chaotic advection. Based on a theoretical analysis, *Lester et al*. [2010] proposed a temporally rotating dipole setup. *Piscopo et al*. [2013] developed an optimal sequence for a five spot configuration. *Zhang et al*. [2009] used an oscillatory pumping scheme of three wells randomly located with some realistic constraints to avoid dewatering and preserve mass.

The effect of heterogeneity implied the increase of mixing from chaotic advection. Most of the works focused on physical mixing [*Lester et al*., 2010; *Zhang et al*., 1996] and at most involved simple reactions. For example, *Piscopo et al*. [2013] analyzed the formation of one product by the instantaneous reaction of two reagents, following a 1:1 stoichiometry. They found that chaotic advection might improve the reactivity of some compounds by a factor of 5, but did not evaluate the interaction between geochemistry and flow dynamics.

In this context, we should note that the degradation of macro and micropollutants typically follow complex nonlinear geochemical processes, including noninstantaneous homogeneous or heterogeneous (in terms of phases involved) reactions. In the case of EOCs, degradation might be driven, mostly, by cometabolic processes characterized by secondary reactions. One example of this complex network of reactions is the degradation of three compounds: benzotriazole (BT), 5-methyl-benzotriazole (TRI), and 5-chloro-benzotriazole (CBT). These are common compounds in groundwater, as conventional wastewater treatment do not remove them completely [*Alotaibi et al*., 2015]. The individual degradation of benzotriazole compounds depends on redox conditions [*Liu et al*., 2013]; aerobic conditions favor the degradation of BT and TRI, while CBT is preferentially degraded under anaerobic conditions.

Based on this, the main goal of this work is to evaluate the enhancement of the degradation of three benzotriazoles compounds in a heterogeneous porous media associated to the implementation of an injection/extraction setup linked to a MAR-SAT system resulting in chaotic advection. As a secondary goal, we further analyze the changes in the spatial distribution of redox zonation associated with the pumping scheme.

2. Model Description

2.1. Setup

To achieve the main goals of this work, we performed synthetic models. We consider a simplified setup with one infiltration pond that operates continuously at a constant rate at specific periods. Four wells are placed around the pond forming a square of side 175 m, and oriented along the north-south and east-west directions (see Figure 1). These wells are assumed to inject and extract groundwater with the engineered sequence reported by *Piscopo et al*. [2013]. This will be also demonstrated here for a MAR-SAT system. In

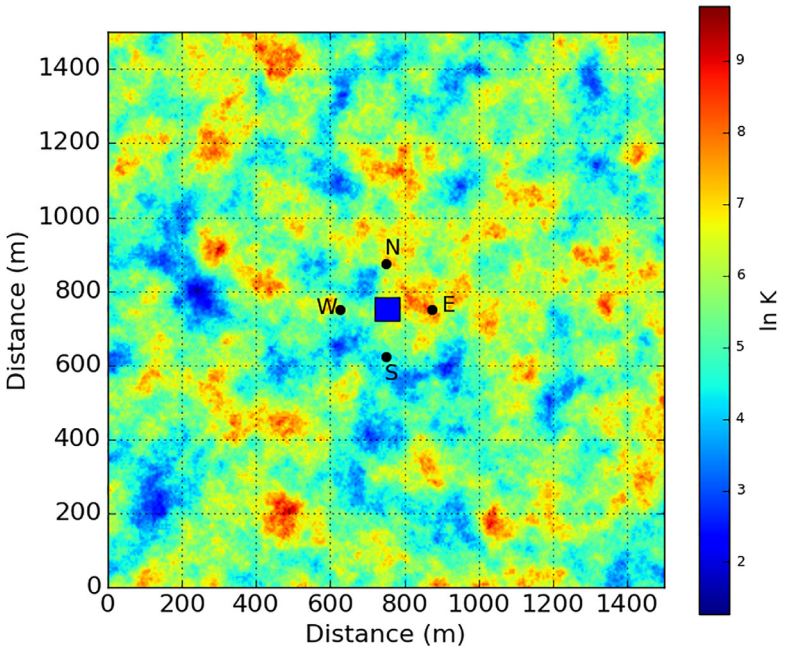

Figure 1. Conceptual model and an example of the heterogeneous hydraulic conductivity field. The black points represent the position of the four extraction wells (North, South, West, and East) around the infiltration pond (blue square).

short, the sequence can be described as follows: first, the east and west wells operate at different injection and extraction flow rates to spread the plume along the west/east direction. The sequence is then repeated with the north and south wells to stretch the plume (see Figure 1). The sequence was modified each 6.25 days. The change of the direction (90°C, from N–S to E–W) pretended to deform the plume by stretching and folding see *Piscopo et al*. [2013]. We considered two different recharging cycles of varying duration (recharge flow was kept constant in the two scenarios): one with 19 days of recharge followed by 19 days of nonrecharge, denoted as scenario E1, and another with 25 days of recharge and 12.5 days of nonrecharge, scenario E2. Thus, in E1 the total recharging days were 56.3, whereas in E2 they were 68.8 days. We followed a discontinuous recharge system because it reduces the risk of clogging [*Rodríguez-Escales et al*., 2016]. Figures 2a and 2b illustrate the recharging cycles and the sequence of well injections and extractions for the two scenarios.

2.2. Flow and Transport Model

We simulated the flow of groundwater and the transport of organic matter, electron acceptors, and a benzotriazole mixture (three compounds) taking place in an underlying coarse sand aquifer associated with a MAR-SAT facility. The rationale, geometry, and the values of the hydraulic parameters were taken from the facility actually operating in the Llobregat Lower Valley near Barcelona, Spain [*Valhondo et al*., 2014].

The model considered a two-dimensional aquifer that extends over an area of 1500 × 1500 m. Constant head values were assigned at the east and west boundaries to simulate a natural head gradient of 2.3×10^{-3} oriented along the *x* direction. No flow conditions were set at the North and South boundaries. The MAR-SAT system is centered in the middle of the aquifer and covers a total squared surface of 4225 m^2.

The aquifer is assumed heterogeneous with a local isotropic transmissivity that varies in space. The governing flow equation is

$$\nabla \cdot (T(\boldsymbol{x})\ \nabla h(\boldsymbol{x},t)) + w(\boldsymbol{x},t) = S\frac{\partial h(\boldsymbol{x},t)}{\partial t}, \tag{1}$$

where $h(\boldsymbol{x},t)$ is the hydraulic head, $T(\boldsymbol{x})$ the transmissivity at the **x** location, *S* the storage coefficient, and w(**x**,t) the source/sink term accounting for the recharging water and the injection and extraction wells. In accordance with real operations of MAR systems [*Greskowiak et al*., 2006; *Valhondo et al*., 2014], we considered a recharge rate of 1 m/d; both the recharge and the pumping sequences are described in Figure 1 and in section 2.1. To avoid flow transient effects, the storage coefficient is set constant and equal to 10^{-5}. Such value corresponds to a characteristic time of 5×10^{-4} days, assuming a homogeneous media with T = 250 m^2/d, indicating that the aquifer would respond almost immediately to any stress (e.g., pumping).

The transport of species is described by the following governing partial differential equation,

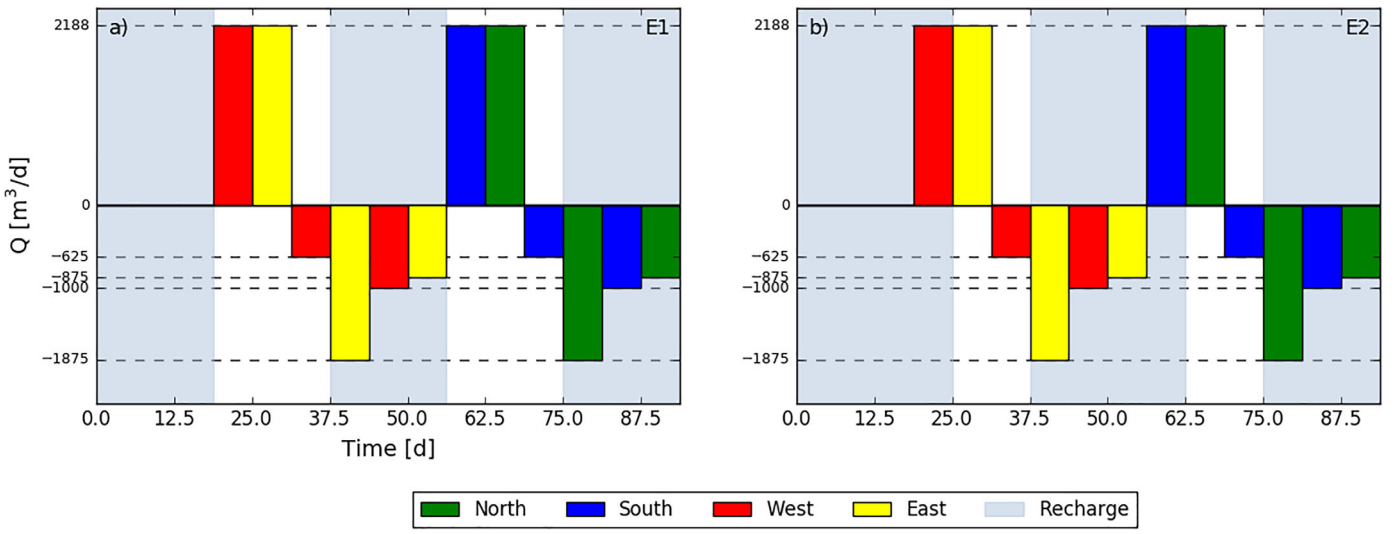

Figure 2. Different scenarios of pumping and recharge. Each scenario is compared in homogenous and in heterogeneous media as well as with and without chaotic advection.

$$-\boldsymbol{q}(\boldsymbol{x},t)\nabla C_i(\boldsymbol{x},t)+\nabla\cdot(\phi\boldsymbol{D}\nabla C_i(\boldsymbol{x},t))+f_i(\boldsymbol{x},t)-\phi r_i(\boldsymbol{x},t)=\phi\frac{\partial C_i(\boldsymbol{x},t)}{\partial t} \quad (2)$$

where C_i is the concentration of the ith species, $q(\boldsymbol{x},t)$ the specific discharge, ϕ is porosity, $\boldsymbol{D}$ the hydrodynamic dispersion tensor, f_i the mass flux source/sink term that accounts for mass extraction and injection from wells or in the recharging water, and r_i the biochemical reaction term that represents degradation. The porosity was set to 0.25, and the longitudinal and transverse dispersivities were fixed at 50 and 5 m, respectively.

The chemical composition of the groundwater in the model was based on the representative hydrochemistry of the Llobregat aquifer [*Valhondo et al.*, 2014], see Table 1. To simplify the system and to avoid secondary reactions that could be induced by mixing of waters with different composition (thus potentially masking the overall effect of chaotic mixing), we assumed that the recharging and the injected water had also the composition in Table 1 except in the former, where dissolved organic carbon (DOC) had a concentration of 5 m*M* to represent that a permeable reactive layer made up of organic matter (mixed with sand in proportion 1:1) was operating at the bottom of the infiltration pond.

Table 1. Hydrochemistry of Both the Initial Groundwater and the Regional Groundwater. (*) Fe^{+3} and Mn^{+4} Were Added as Immobile Species in Their Mineral Form (Goethite and Pyrolusite)[a]

Compound	Unit	Groundwater
BT	M	8.39×10^{-9}
TRI	M	7.59×10^{-9}
CBT	M	6.52×10^{-9}
O_2	M	9.38×10^{-5}
Ca^{2+}	M	3.40×10^{-3}
Mg^{+2}	M	9.63×10^{-4}
Na^{+1}	M	2.20×10^{-3}
K^{+1}	M	1.00×10^{-4}
Cl^{-1}	M	2.10×10^{-3}
NO_3^{-1}	M	1.29×10^{-4}
Fe^{3+} (*)	M	4.29×10^{-4}
Mn^{4+} (*)	M	1.64×10^{-4}
SO_4^{-2}	M	1.20×10^{-3}
DIC	M	8.00×10^{-3}
pH		7
pe		12

[a]The concentration presented in the Table is normalized from solid concentration considering the porosity and the soil density (2.2kg/L).

2.3. Biogeochemical Model: Benzotriazole Mixture Degradation Coupled to Organic Matter Oxidation

The simulation of organic matter (DOC), with a chemical formula of CH_2O, was carried out considering the full Redox sequence which starts with the electron acceptor most energetically favorable (oxygen), followed by anaerobic degradation under the following sequence: nitrate-reducing, manganese-reducing, iron-reducing, and, finally, sulfate-reducing (Table 2).

The full degradation rate of organic matter can be expressed as:

$$r_{DOC}=C_{DOC}\sum_{i=1}^{n}\left(-k_i\frac{C_i}{C_i+K_{sat,i}}\prod_{j=1}^{m}\frac{C_{j,i}+K_{inh,j,i}}{K_{inh,j,i}}\right) \quad (3)$$

where n are the number of the terminal electron acceptors (here oxygen, nitrate,

Table 2. Reduction and Oxidation Sequence Reactions

Geochemical Reaction	Reaction Formula	Gibbs (kcal/mol)
Aerobic oxidation	$CH_2O + O_2 \rightarrow HCO_3^- + H^+$	−120
Denitrification	$CH_2O + 0.8\,NO_3^- + 0.8\,H^+ \rightarrow HCO_3^- + 0.4\,N_2 + H^+ + 0.4H_2O$	−114
Manganese reduction	$2CH_2O + 4MnO_2 + 6\,H^+ \rightarrow 2HCO_3^- + 4Mn^{2+} + 4\,H_2O$	−81
Iron reduction	$CH_2O + 4FeO(OH) + 7\,H^+ \rightarrow HCO_3^- + 4Fe^{2+} + 6\,H_2O$	−28
Sulfate reduction	$2CH_2O + SO_4^{-2} \rightarrow 2HCO_3^- + HS^- + H^+$	−25

pyrolusite, goethite, sulfate, and methane), C_i [M/L^3] are the concentrations with respect to each terminal electron acceptor; k_i [T^{-1}] and $K_{sat,i}$ [M/L^3] are, respectively, the rate and the half-saturation constants with respect to each terminal electron acceptor, m are the number of inhibition species (oxygen, nitrate, pyrolusite, goethite, and sulfate), $C_{i,j}$ [M/L^3] are the concentrations with respect to each inhibition species in the electron acceptor reaction; and $K_{inh,j,i}$ [M/L^3] are the inhibition constants for species j and reaction i. The constants were taken from *Rolle et al*. [2008] and compared well with similar works in the literature on organic matter oxidation [*Brun and Engesgaard*, 2002; *Greskowiak et al*., 2006; *Mayer et al*., 2001; *Prommer and Stuyfzand*, 2005; *Prommer et al*., 2002; *Prommer et al*., 2006; *Rolle et al*., 2008].

The degradation rates of benzotriazole (BT), 5-methyl-benzotriazole (TRI), and 5-chlorobenzotriazole (CBT) were considered to depend on redox conditions as described by *Liu et al*. [2013], who evaluated the individual degradation of these three compounds in aquifer material under four different redox conditions (aerobic and anaerobic-nitrate-reducing, sulfate-reducing, and iron-reducing conditions). Based on this, the degradation of BT, TRI, and CBT were simulated using the following first-order kinetic reaction,

$$r_j = -C_j \sum_{i=1}^{n} k_{j,i} F_i j = BT, TRI, CBT \tag{4}$$

where *i* represents the redox condition, up to the *n* ones where benzotriazoles degradation was studied, and $k_{j,i}$ [T^{-1}] was the first-order degradation constant for each species *j* at a specific redox state. These $k_{j,i}$ values were obtained from the work of *Liu et al*. [2013], and shown in Table 4. Since different redox conditions occurred simultaneously in the aquifer during the simulations, we incorporated in (4) the activation factors F_i, which is a binary process equal to 1 when the redox process i is active at a given location, and

Table 3. Parameters Used in the Reactive Transport Model: Maximum Degradation Rates (k), Half-Saturation Constants (K_s), and Inhibition Constants (K_i)

Parameter		Unit	This Work	Literature	Ref.
K	O_2	d^{-1}	0.15	0.15[a], 0.08[a], 0.01[b]	[a,b]
	NO_3^-	d^{-1}	0.12	0.12[a], 0.01[a], 0.001[b]	[a,b]
	FeOOH	d^{-1}	0.11	0.11[a], 0.008[a]	[a,b]
	MnO_2	d^{-1}	0.1	0.10[a], 0.011[a], 0.0002[b]	[a,b]
	SO_4^{2-}	d^{-1}	0.09	0.09[a], 0.12[a], 0.01[b]	[a,b]
	CO_2	d^{-1}	0.08	0.08[a], 0.6[a], 0.001[b]	[a,b]
K_S	O_2	M	1.56×10^{-5}	1.56×10^{-5}[a], 1.00×10^{-5}[c], 3.1×10^{-6}[d], 2×10^{-3}[e], 2.94×10^{-4}[f]	[a,c,d,e,f]
	NO_3^-	M	8.06×10^{-6}	8.06×10^{-6}[a], 1.00×10^{-5}[c], 8.1×10^{-6}[d], 1.55×10^{-4}[f]	[a,c,d,f]
	FeOOH	M	5.75×10^{-6}	9.09×10^{-6}[a], 2.4×10^{-4}[d], 1.00×10^{-4}[f]	[a,d,f]
	MnO_2	M	5.62×10^{-6}	8.93×10^{-6}[a]	[a]
	SO_4^{2-}	M	5.21×10^{-6}	5.21×10^{-6}[a], 1.6×10^{-4}[d], 1.00×10^{-5}[e]	[a,d,e]
	CO_2	M	3.13×10^{-5}	1.14×10^{-5}[a]	[a]
K_I	O_2	M	3.13×10^{-7}	3.13×10^{-7}[a], 1.00×10^{-5}[c], 3.1×10^{-5}[d]	[a,c,d]
	NO_3^-	M	1.61×10^{-7}	1.61×10^{-7}[a], 1.6×10^{-5}[d]	[a,d]
	FeOOH	M	1.15×10^{-7}	1.82×10^{-7}[a]	[a]
	MnO_2	M	1.12×10^{-7}	1.79×10^{-7}[a]	[a]
	SO_4^{2-}	M	1.04×10^{-7}	1.04×10^{-7}[a]	[a]

[a]*Rolle et al*. [2008]; [b] *Brun and Engesgaard* [2002]; [c] *Greskowiak et al*. [2006]; [d] *Mayer et al*. [2001]; [e] *Prommer et al*. [2002]; and [f] *Prommer et al*. [2006].

Table 4. Parameters Used in the Reactive Transport Model for the Degradation of Benzotriazole and Its Derivative Compounds[a]

Compound	Condition	k	Unit
Benzotriazole (BT)	O_2	0.0161	d^{-1}
	NO_3^-	0.091	d^{-1}
	FeOOH	0.0147	d^{-1}
	SO_4^{2-}	0.0084	d^{-1}
5-methyl-benzotriazole (TRI)	O_2	0.0221	d^{-1}
	NO_3^-	0.0115	d^{-1}
	FeOOH	0.0177	d^{-1}
	SO_4^{2-}	0.0091	d^{-1}
5-chlorobenzotriazole (CBT)	O_2	0.0147	d^{-1}
	NO_3^-	0.0329	d^{-1}
	FeOOH	0.0211	d^{-1}
	SO_4^{2-}	0.0128	d^{-1}

[a]All parameters were taken from *Liu et al*. [2013].

zero otherwise. Note that microorganisms mediate all the degradation processes described above. Nevertheless, in this work we did not consider neither the growth nor the decay of biomass, which is assumed sufficiently large and effectively constant.

2.4. Methodology

A stochastic framework is used to account for the spatial variability of the transmissivity (T) field. Here T is described as a random space function, which renders the flow and transport equations stochastic. The natural log of the transmissivity, denoted as $Y(\boldsymbol{x}) = \ln T(\boldsymbol{x})$, is considered to follow a multi-Gaussian random process characterized by an isotropic spherical covariance function with a mean of 5.52, a variance of 5, and an integral scale of 70.9 m. The numerical experiment is embedded in a Monte Carlo framework, consisting of five sequential steps: (1) simulation of equilikely transmissivity fields; (2) solving the flow problem associated to each T field; (3) solving the reactive transport problem for each transient flow solution to map the redox zonation as a function of space and time; (4) estimating the concentration of benzotriazoles from first order degradation, and (5) estimating the statistics of key variables at different times.

A total of 300 random transmissivity fields were generated with the sequential Gaussian simulation algorithm available in SGeMS [*Deutsch and Journal*, 1992]. This setup leads to a range of transmissivities that spanned more than 3 orders of magnitude around the geometric mean value of 250 m^2/d (the homogeneous field with T = 250 m^2/d was also analyzed as a reference case). In each simulation, the flow equation was solved using the finite differences code, Modflow-2005 [*Harbaug*, 2005], with a domain discretized in square cells of size 25 m^2.

The reactive transport problem was also solved using a finite differences code, PHT3D v2.17 [*Prommer and Post*, 2010]. This code has been thoroughly used to simulate the evolution of groundwater chemistry during organic matter degradation and was successfully benchmarked [*Prommer et al*., 2003] and applied to different network degradation reactions similar to that in (4) [*Greskowiak et al*., 2006; *Prommer et al*., 2006; *Rodríguez-Escales et al*., 2016]. PHT3D couples the transport simulator MT3DMS [*Zheng and Wang*, 1999] and the geochemical code PHREEQC-2 [*Parkhurst and Appelo*, 1999] using a sequential splitting-operator technique. For reactions in equilibrium, the constants were taken directly from the basic database of PHREEQC-2. Kinetic reactions comprising degradation of organic matter and those of benzotriazole and its derivatives (TRI and CBT), not being part of the standard database, were incorporated into the module in the form of BASIC routines. The total simulation time was 93.75 days with a time discretization of 0.31 days. The transport equation was solved using the TVD scheme.

3. Results and Discussion

3.1. Evaluating the Effect of Chaotic Flow in Physical Mixing

We started by evaluating the enhancement of mixing due to chaotic flow (Figure 3). This was based on a conservative tracer added to the recharged solution at a concentration of 5 m*M*. The Dilution Index [*Kitanidis*, 1994], denoted here as DI, is used as a performance metric. DI measures the departure of the particle distribution within the full domain from the uniform distribution. The mass of tracer in each cell is

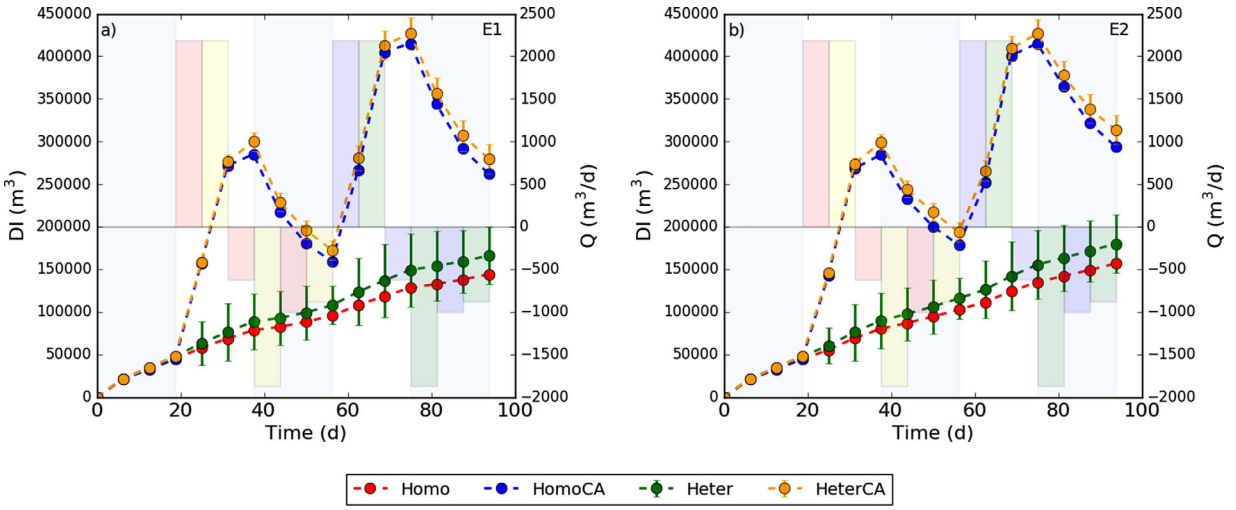

Figure 3. Dilution Index (DI) in (a) scenario 1, E1, and (b) scenario 2, E2. Pumping sequence is diluted behind plot for visibility.

obtained from the simulations and normalized by the total injected mass, indicating the probability that a tagged particle is found in a given grid cell. The Dilution Index is thus a measure of the entropy of the spatial distribution of particles [*Chiogna et al*., 2012; *Kitanidis*, 1994]. As shown in Figure 3, after chaotic flow started (at day 17.25) DI increased considerably, explained by the superposition of streamlines promoted by the sequence of injection and extraction, allowing the contact (and further mixing) between the two solutions. The increase in DI was quite similar in both recharging scenarios considered (Figures 3a and 3b), indicating that the recharge protocol did not affect mixing.

On the other hand, the pumping sequence had an important impact upon the dilution index. The variation of DI matched in time with pumping sequence; DI decreased when extraction occurred, and increased during injection periods, linked again to entropy concepts. Thus, extraction implied a reduction of system entropy, meaning that mixing was overall much improved with chaotic flow. At the end of the pumping sequence, there was a factor of 2 (locally up to 3) improvement as compared with the scenarios without chaotic flow. We want to emphasize that we have evaluated the effect of mixing in 2-D; in the reality (3-D) dilution is expected to be larger [*Ye et al*., 2015].

3.2. Evaluating the Effect of Chaotic Flow in the Redox Zonation

Once corroborated that physical mixing was improved by chaotic flow, we analyzed the consequences upon the temporal distribution of the redox zonation. As a first step, we analyzed how the surface area of the zones corresponding to the different redox processes increased with time. This value was determined by counting the grid cells with a given redox activity. Two thresholds of degradation rates of TEAPs were considered, with activities or rates values higher than 10^{-15} (representing the zone with a high activity, i.e., the hotspots), and 10^{-30} Ms^{-1} (little restrictive, so that it that can be used to delineate the total area corresponding to a given redox zonation).

Figure 4 shows that after pumping started, the surface area, measured in m^2, corresponding to redox states increased considerably in both scenarios evaluated (with the exception of sulfate-reduction).

The increasing of the surface for the two thresholds indicated that when the sequence of injection extraction was activated, both the spreading of redox processes and the total reacted mass were enhanced. Furthermore, the moles of total reaction for the different electron acceptors for each redox process was also higher at the end of the pumping cycle in the scenarios with chaotic flow (Table 5), confirming that the chaotic flow results in an increase in total reactivity with a factor of more than 2 for all redox processes with the exception of sulfate (discussed below). This is noticeable since this enhancement was achieved also in manganese and iron-reducing conditions even though the water used both for recharge and injection was aerobic. Notice that the extracted water was not recirculated into the injection wells as this option is not legal in many countries in the world.

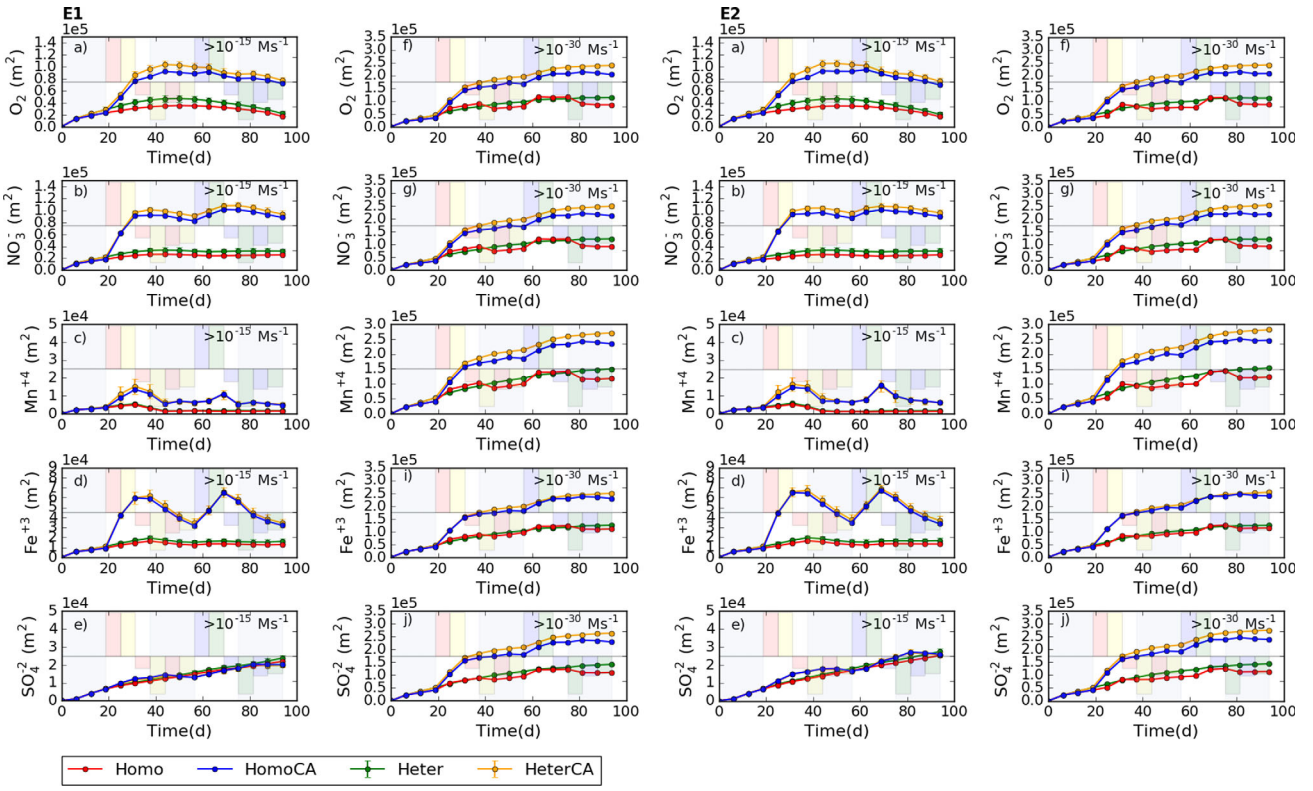

Figure 4. Occupied surface by different redox rates at different thresholds (values higher than 10^{-15} and 10^{-30} Ms^{-1}) in (a–j) scenario E1, and (a′–j′) scenario E2.

The increase in organic matter (OM) degradation is a combination of the variability of the redox processes and the reactivity of OM for a given redox condition, displayed in Table 5 as integrated values. Figure 5 shows the spatial distribution of hotspots of the different terminal electron-accepting processes (TEAPs) for the homogeneous case in scenario E1 (the values were similar for scenario E2). The behavior in the heterogeneous one was evaluated in individual realizations (an example is provided in the supporting information as a movie (ms01), to see the variation in time). In the scenarios without chaotic flow (Figure 5), the dominating redox condition, in terms of occupied surface-area, are oxygen and nitrate reduction, while when chaotic flow was applied a larger variability in the redox conditions was observed (oxygen, nitrate, manganese, and sulfate reduction).

There was no significant change in the increasing of the surface in the two scenarios evaluated (Figures 4a and 4b). Nevertheless, the total amount of electron acceptors degraded was higher for all TEAPs in scenario E2. This is explained because E2 implied a higher period of recharge and, thus, a higher amount of organic carbon supplied to the system as compared to E1.

Sulfate had a singular behavior compared to the other electron acceptors: for the highest threshold (10^{-15} Ms^{-1}), the surface was similar in all cases evaluated (Figures 4a and 4b) and the total degraded mass was also similar (slightly larger in the scenarios without chaotic flow, Table 5). This is explained because the initial concentration of sulfate was quite higher than those of the other electron acceptors (around 1 order of magnitude compared to nitrate and oxygen, Table 1). As organic matter was not limiting, sulfate reduction occurred without limitation. Although the reduction of the others TEAPs was more thermodynamically favorable, as their concentrations were lower, the total amount of degraded moles was also lower. These low concentrations of oxygen and nitrate promoted that these two TEAPs in the recharged solution were easily degraded, on the other hand, as sulfate concentration was higher it remained in that solution. Therefore, the subsequent degradation of oxygen and nitrate depended on the mixing between the recharged solution (rich in OM) and groundwater, being a fringe-controlled degradation.

Actually, sulfate degradation occurred both in the recharged water itself (there was electron donor and sulfate) and by fringe control, but, as higher concentrations of OM were present in the recharged water, the

Table 5. Total Moles Degraded of Different Terminal Electron Acceptors and Benzotriazoles After One Chaotic Flow Cycle (93.75 days) With and Without Chaotic Flow in Scenario 1[a]

	SCENARIO E1					
	Homogenous (Degraded Moles)		Heterogeneous (Degraded Moles)			
TEAPs and EOCs	Without Chaotic Flow	With Chaotic Flow	Without Chaotic Flow (mean + SD)		With Chaotic Flow (mean + SD)	
Oxygen	45.25	88.25 (×1.95)	52.25	8.75	110.50 (×2.11)	28.25
Nitrate	686.50	1921.50 (×2.80)	790.75	145.00	1987.75 (×2.51)	363.00
Manganese	2162.00	2942.50 (×1.36)	2159.00	206.75	3037.50 (×1.41)	549.00
Iron	203.00	410.25 (×2.02)	227.50	69.25	458.00 (×2.01)	189.50
Sulfate	27350.00	27325.00 (×0.87)	27325.00	250.75	23705.00 (×0.87)	1312.75
Benzotriazole (BT)	1.97×10^{-1}	2.16×10^{-1} (×1.99)	2.16×10^{-1}	2.24×10^{-2}	3.97×10^{-1} (×1.83)	4.02×10^{-1}
5-methyl-benzotriazole (TRI)	1.81×10^{-1}	3.8×10^{-1} (×2.09)	2.05×10^{-1}	2.05×10^{-2}	3.85×10^{-1} (×1.92)	3.97×10^{-1}
5-chlorobenzotriazole (CBT)	1.69×10^{-1}	4.45×10^{-1} (×2.63)	1.90×10^{-1}	2.33×10^{-2}	4.50×10^{-1} (×2.37)	4.97×10^{-1}
	SCENARIO E2					
Oxygen	44.75	90.00 (×2.01)	52.00	8.75	113.00 (×2.17)	30.75
Nitrate	682.25	2179.25 (×3.20)	787.75	131.25	2227.25 (×2.82)	377.75
Manganese	2193.00	3380.00 (×.154)	2202.00	212.5	3495.00 (×1.59)	646.5
Iron	194.50	467.75 (×2.40)	215.25	63.75	510.00 (×2.37)	177.75
Sulfate	34050.00	30025.00 (×0.88)	34025	277.25	29950.00 (×0.88)	1365.5
Benzotriazole (BT)	2.16×10^{-1}	4.78×10^{-1} (×2.21)	2.37×10^{-1}	2.39×10^{-2}	4.85×10^{-1} (×2.05)	5.10×10^{-2}
5-methyl-benzotriazole (TRI)	1.98×10^{-1}	4.63×10^{-1} (×2.34)	2.18×10^{-1}	2.28×10^{-2}	4.68×10^{-1} (×2.14)	4.95×10^{-2}
5-chlorobenzotriazole (CBT)	1.81×10^{-1}	5.25×10^{-1} (×2.90)	2.05×10^{-1}	2.43×10^{-2}	5.33×10^{-1} (×2.60)	5.88×10^{-2}

[a]The value in brackets represent the improvement of degradation by chaotic flow.

highest rates were observed in the latter (see Figures 5a and 5b). As the center of the plume was less affected by the injection and extraction sequence and as the highest rates of sulfate were in the recharged solution and not in the fringes, it seems logical that the highest rates of sulfate were similar in all the cases and independent on chaotic flow (Figure 4a and 4b). Furthermore, as recharge was semicontinuous, there was not enough time to allow complete mixing of sulfate.

Besides this, chaotic flow enhanced the degradation of manganese and iron, only present in mineral form, and not in the recharged water. Their degradation was thermodynamically limited by that of nitrate and oxygen that were fringe limited. This is confirmed because the surface of the hotspots of manganese and iron followed the pumping sequence, indicating that the degradation of these two TEAPs was highly enhanced by chaotic flow.

All the increases in reactive rates were, then, related to the enhanced mixing produced in the fringes delineating zones promoted by chaotic flow. Under natural flow and as a general statement, biodegradation processes (e.g., organic matter degradation) are most pronounced at the plume fringe, as microbial activity focuses on a narrow mixing zone along the fringes, where dissolved electron acceptors and donors are mixed by transverse dispersion [*Chu et al*., 2005; *Cirpka et al*., 1999; *De Simoni et al*., 2007]. It has been established that when a transient flow occurs (induced by pumping or driven by heterogeneity), this mixing effect is enhanced [*Bauer et al*., 2009; *Prommer et al*., 2002; *Schirmer et al*., 2001; *Werth et al*., 2006]. Chaotic flow creates a highly transient flow through the superposition of streamlines; this facilitated the contact between the electron donors, present in the recharge water, with the electron acceptors, present in groundwater. Note that all the reactions of organic matter degradation are mediated by microorganisms; in this work, we have considered that microorganism activity was not a limitation to the degradation being constant and not affected by chaotic flow. In this way, future research is needed to evaluate the effect of chaotic flow in microorganism dynamics.

3.3. Evaluating the Effect of Chaotic Flow in the Degradation of Benzotriazoles

Following the same methodology as in the previous section, we evaluated the evolution in time of the surface where individual benzotriazoles were degraded in a rate exceeding a given threshold (Figures 6a and 6b). The surfaces increased at all thresholds evaluated (the figures report 10^{-15} and 10^{-30} Ms^{-1}) and for all three evaluated compounds (5-chlorobenzotriazole (CBT), 5-methyl-benzotriazole (TRI), and benzotriazole (BT)). Chaotic flow increased the total degraded moles in the two scenarios evaluated, from a factor of 1.8 to 2.4 in scenario E1, and 1.6 to 2.6 in scenario E2 (Table 5). This slight improvement observed in E2 was

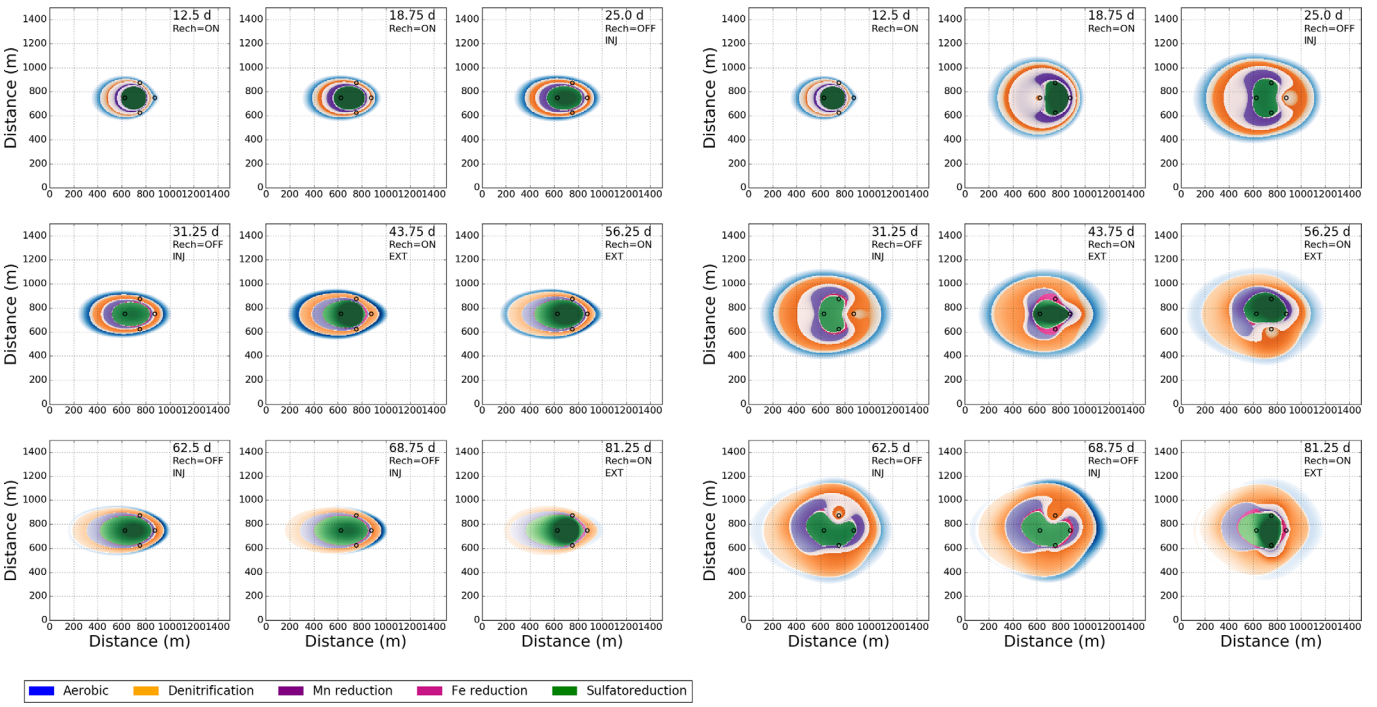

Figure 5. Hotspot ($>10^{-15}$ Ms^{-1}) of different redox rates (in logarithmic form) at different times in homogenous media (a) without chaotic flow (E1), and (b) with chaotic flow (E1). Intensity of colors is proportional to the rate value. "Rech." refers to Recharge, "INJ" to Injection, and "EXT" to Extraction.

explained by the longer recharge period in this case, implying a higher amount of organic matter supplied to the system, thus facilitating the cometabolic degradation of all benzotriazoles. Notice that the surfaces reported for all three compounds were somewhat different from those corresponding to the terminal

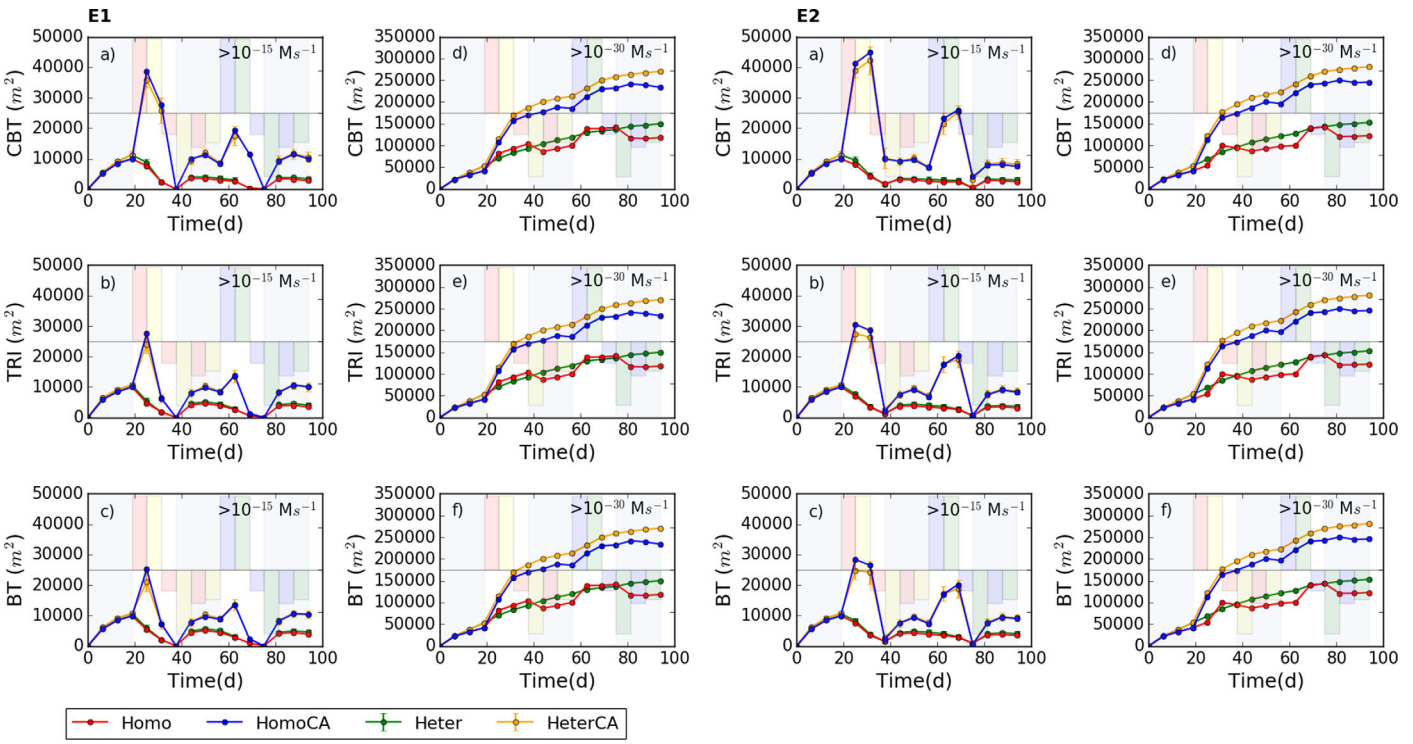

Figure 6. Occupied surface by different benzotriazoles rates (in logaritmic form) at different thresholds (values higher than 10^{-15} and 10^{-30} Ms^{-1}) in (a–f) scenario E1, and (a′–f′) scenario E2.

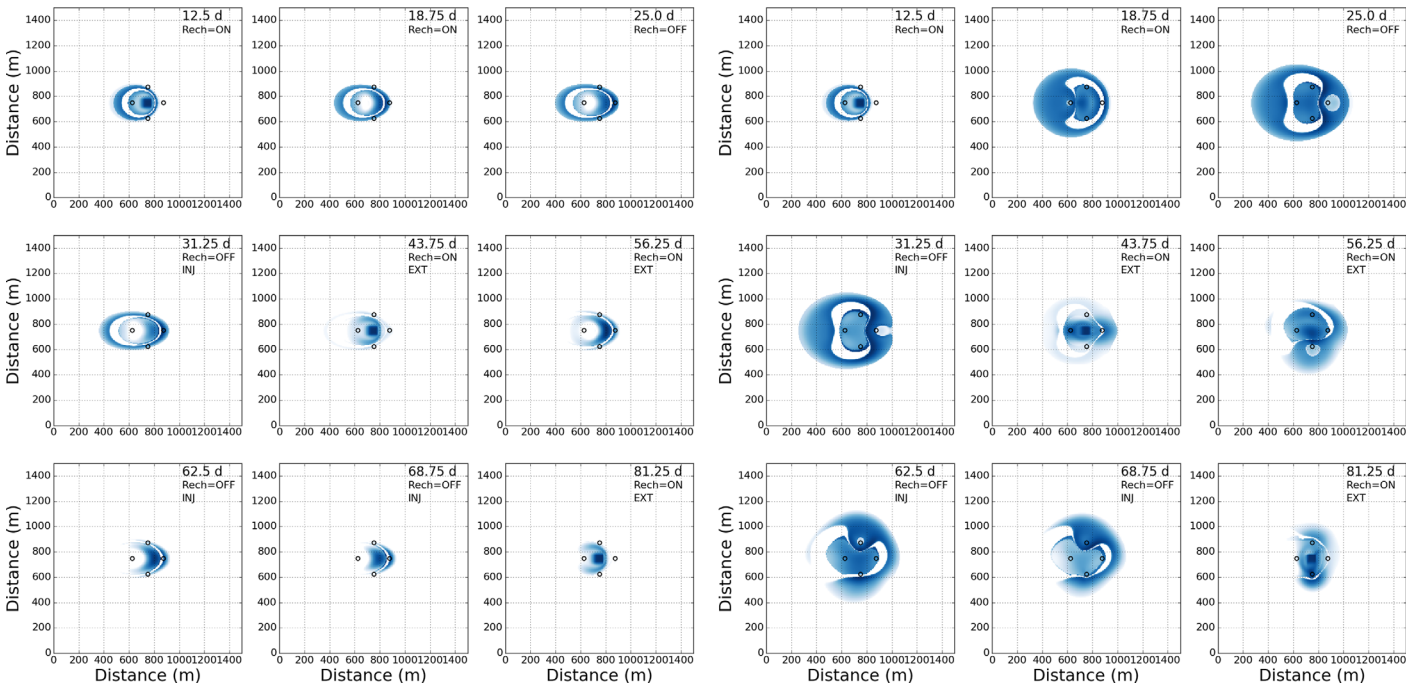

Figure 7. Hotspot ($>10^{-15}$ Ms^{-1}) of CBT at different times in homogenous media for scenario E1, (a) without chaotic flow, and (b) with chaotic flow. Intensity is proportional to rate.

electron acceptors. Whereas for the TEAPs the surface increased in the injection periods and decreased during extraction, (similar to DI), the EOCs were mostly dependent on recharge; more precisely on the amount of organic matter supplied. Note that the behavior of TRI and BT were quite similar, as they both are best degraded under aerobic conditions, while CBT degrades preferentially under nitrate-reducing conditions.

Figures 7a and 7b display the temporal evolution of the CBT plume as an example of overall behavior of EOCs. They show how hotspots of degradation were heavily influenced by the recharge episodes: when it was activated, the degradation hotspot were centered below the infiltration pond, whereas in the no recharge episodes, and especially during injection, the hotspots were located in the fringes. In the case of CBT, as nitrate-reducing condition was the best for degradation, the hotspots matched with those of nitrate degradation. Notice that no degradation was taking place in the zone of manganese reduction, since benzotriazoles are not degraded under this specific redox condition [see *Liu et al*., 2013].

Overall, the application of chaotic flow improved the degradation of all benzotriazoles mixtures independently of the redox conditions under which they are preferentially degraded, because they were all occurring simultaneously. In the scenarios without chaotic flow, CBT was the less degraded EOC because the system was mostly under aerobic conditions. The inclusion of chaotic flow implied an enhancement of anaerobic processes (e.g., nitrate reduction) and resulted CBT to be the most degraded benzotriazole. We conclude that in order to achieve the optimal degradation of a EOCs mixture in an infiltration pond, it is quite desirable to have a high variability of redox processes and to increase it extension and reactivity, which can itself be achieved by applying chaotic flow. To date, over 200 different EOCs have been reported in river waters globally [*Hughes et al*., 2013] and each compound has its own particularities for its degradation. It is clear to us that achieving the optimal degradation conditions for all compounds simultaneously is not viable. In addition, although efforts are underway to understand the degradation pathways of many EOCs [*Rodríguez-Escales and Sanchez-Vila*, 2016], most of them are still unknown. For this reason, we contend that the most intelligent management for the degradation of a wide variety of EOCs is a broad-spectrum strategy, such as the application of chaotic flow, which may result in the presence of multiple redox conditions within a single domain.

3.4. Time Evolution of Degradation Rates and Demonstration of Achieving Full Mixing

We analyzed the time evolution of total degraded mass of the benzotriazole mixture, *R*, in a log-log plot (Figure 8, we only show the results for E1 as no differences were observed between the two scenarios). For

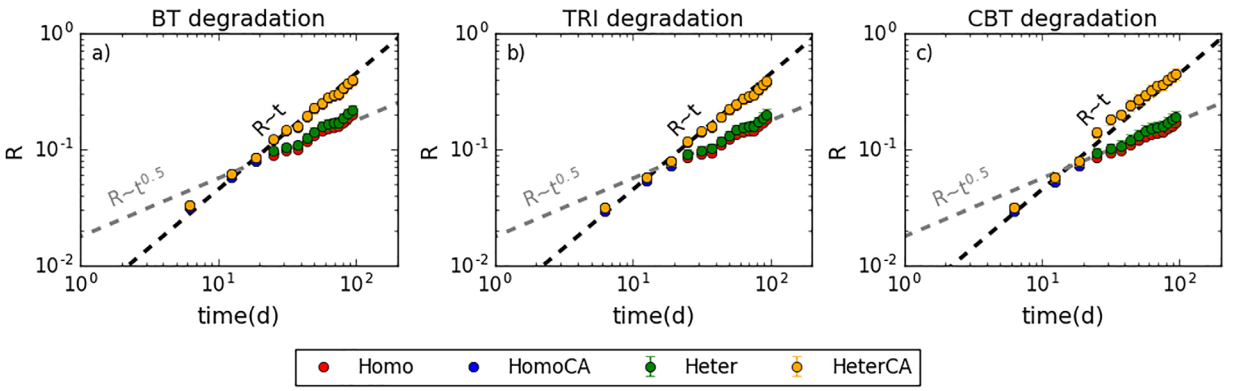

Figure 8. Evolution of the coefficient of variation of the dilution Index in (a) Scenario 1 and (b) Scenario 2.

all benzotriazoles, total reaction was significantly different depending on whether chaotic flow was applied. In the absence of chaotic flow, there is a transition from a slope of 1, implying that $R \approx t$ for small time values, to a nonlinear behavior with a characteristic slope of $^1/_2$ (i.e., $R \approx t^{0.5}$). On the other hand, when chaotic flow is activated, the slope of 1 remains during the full simulation time.

We explain this behavior as follows; it is known that in a one-dimensional system, if full mixing is achieved and if the pollutant is degraded under first-order, the total degraded mass grows with the square root of time [*Gramling et al*., 2002]. Rather, when first-order degradation occurs in a radial system it can be shown that the degraded mass grows linearly with time (see Appendix A). In the analysis performed, degradation of all three benzotriazoles was redox-dependent (and based on the F_i terms in equation (4)). As these terms were binary (0 or 1) and EOCs were ubiquitous in the system, the degradation was assumed instantaneous and first-order.

Then, in the no chaotic flow scenario, there is a transition in the behavior, from the radial flow conditions at short times, characteristic of the infiltration from a pond, and tends asymptotically to a linear recharge behavior (1-D characteristic) as the plume travel mostly controlled by a regional uniform (in the mean) flow. In the scenarios involving chaotic flow, transport is mainly driven by the continuous injection operation, so that the behavior resembles that of radial flow, and the asymptotic regime is never reached.

3.5. Evaluating the Relationship Between Degraded Moles and the Dilution Index

As demonstrated above and in the literature [*Chiogna et al*., 2012; *Dentz et al*., 2011; *Kitanidis*, 1994; *Rolle et al*., 2009; *Werth et al*., 2006], in the case of fast reactions, rates are driven by the availability of the two reactants, caused by mixing. As far we know, it has never been reported how this relationship is modified by chaotic flow. Figure 9 shows the relationship between the total degraded moles of all TEAPs and EOCs with the DI integrated in time. In all TEAPs except sulfate, it was found that when no chaotic flow was imposed, the relationship between these two variables increased rapidly until stabilization of degraded moles. On the other hand, when chaotic flow occurred, this relationship was not stabilized in time, and kept increasing during all the simulated period (Figure 9). Furthermore, this relationship was higher in chaotic flow scenarios, showing that for a same accumulated dilution, more moles were degraded. This is quite logical since we are accounting for accumulated variables. The nonstabilization observed in Figure 9 under chaotic flow conditions could indicate that the maximum degradation of the TEAPs was not achieved, but rather there was still potential for further degradation.

Again, sulfate behaved differently; the total reaction did not stabilize for large DI values, and moreover, it was highest in the case without chaotic flow. As discussed above, this is explained because sulfate degradation did not take place in fringes and it was then somewhat independent of chaotic flow. In any case, local stabilization could be observed in the no recharge periods. That would mean that although the DI increased, the total degraded moles not, confirming that this degradation was not fringe-controlled and it was taking place mainly in the center of the plume of recharged water.

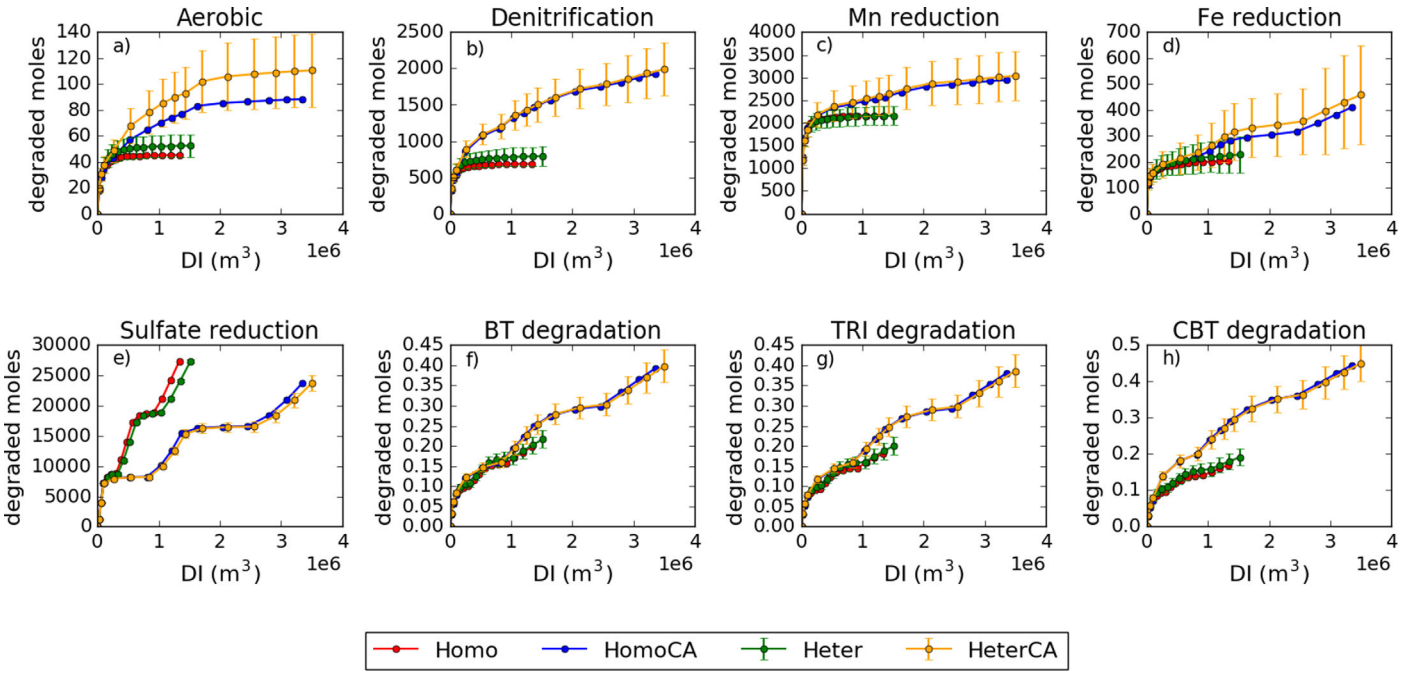

Figure 9. Relationship between degraded moles and accumulated Dillution Index.

Related to the EOCs relationships, the results show that whereas the relationship was higher in the chaotic flow scenarios, the stabilization was not achieved in any case. This could indicate that more time would be needed to achieve a stabilization in total reaction as a function of Dilution Index.

3.6. Uncertainty in Degradation Rates

Monte Carlo simulations allowed evaluating the statistical variability in different observables. In this way, we evaluated how the coefficient of variation (CV) of the Dilution Index (Figure 9) and of the reactive surfaces (Figure 10) is modified by chaotic flow. Results show that CV_{DI} is drastically diminished when chaotic advection is applied. Whereas CV_{DI} in the scenarios that involve chaotic flow was kept more or less constant at a value of 0.05, in the absence of chaotic flow this value raised to values in the order of 0.30–0.45, implying that chaotic flow homogenized the flow system. Although this finding was only evaluated in a medium heterogeneity field ($\sigma^2_{\ln T}=1$), it has relevant implications since activating chaotic flow could blur the relevance of heterogeneity in mixing problems. In this way, further research is needed to evaluate the effect of chaotic flow upon highly heterogeneous scenarios involving the presence of preferential paths. Note that this effect of low CV_{DI} value associated to chaotic flow is a direct consequence of the interaction between chaotic

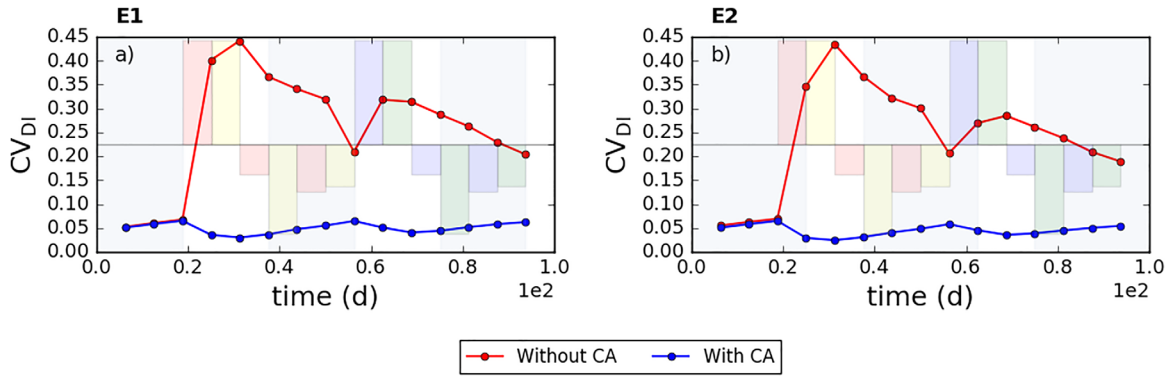

Figure 10. Evolution of the coefficient of variation of Dilution Index in (a) E1 and (b) E2.

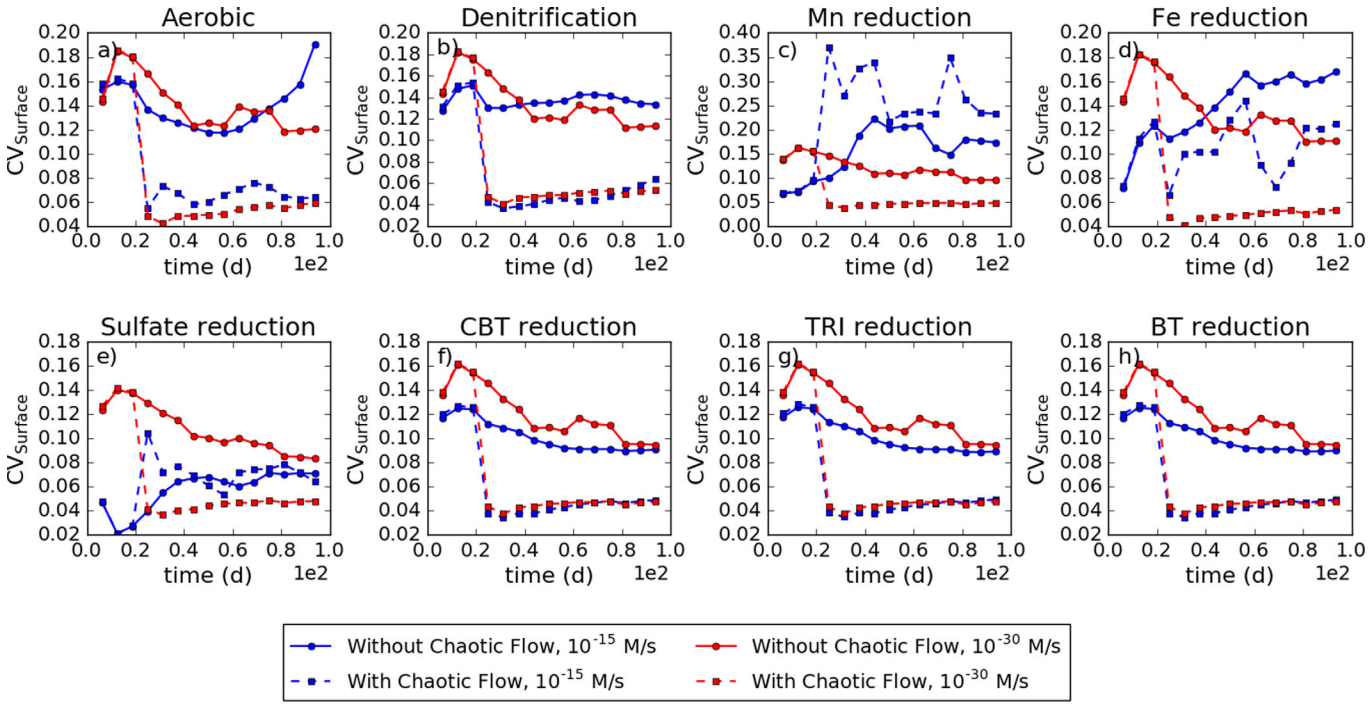

Figure 11. Evolution of the coefficient of variation of TEAPs and EOCs in (a) E1 and (b) E2.

advection and local dispersion; a different result would have been obtained if a pure advection had been considered [*Neupauer et al.*, 2014].

Regarding the effect of chaotic flow in the CV of the reactive compounds (TEAPs and EOCs), in general, the surfaces with rates higher than 10^{-30} Ms^{-1} presented a much lower CV in the scenarios involving chaotic flow (Figure 10). This is consistent with the fact that all the lower rates were governed by chaotic flow since small concentrations of all TEAPs were spread into the system.

In the case of the surfaces of the hotspots (rates higher than 10^{-15} Ms^{-1}), the spatial trends were redox dependent. Nitrate and oxygen had a similar one, confirming that their degradation could be associated to the fringe control of soluble compounds. In the case of Manganese, the hotspots surface in the chaotic flow scenario showed more heterogeneity, whereas in the case of Iron, the CV was lower in the scenarios with chaotic flow. For sulfate, where no important differences in reactive surface and degraded moles were observed, the CV was quite similar in the two scenarios (in the higher rates), indicating that chaotic flow did not modify the homogeneity of sulfate degradation. Finally, the EOCs also show that chaotic flow diminished the variance of the system.

To sum up, chaotic flow homogenized the system in terms of mixing and of reactive surface. This can be explained because the transport was mainly dominated by advection created by pumping sequence instead of dispersion induced by heterogeneity. Thus, heterogeneity played a lower role into the transport and the contact between the two solutions (and mixing) was less dependent, which homogenized the system.

4. Conclusions

In this work, we demonstrated that applying chaotic flow in a MAR-SAT technology would increase the degradation of a benzotriazole mixture. This enhancement is a consequence of the improvement on the physical mixing and on the reactivity of most redox processes by chaotic flow. This improvement in mixing and reaction was evaluated through the Dilution Index, which increased in the scenarios where chaotic flow was implemented. Chaotic flow promotes the contact of the two solutions increasing the mixing and, thus, the dilution and the degradation.

The increase in DI implied also an increase in the reactivity of most Terminal Electron Acceptors (with the exception of sulfate) in at least a twofold factor. Chaotic flow increased the variability of redox process in a given domain, increasing its extension and reactivity. The degradation under oxygen, nitrate, manganese, and iron-reducing conditions was fringe-controlled. Sulfate degradation occurred mostly in the recharged solution, without interaction with groundwater. This is a particularity of Llobregat river water, with high sulfate concentration. For waters with lower sulfate concentration, the degradation is expected to be fringe-limited for all terminal electron acceptors.

The direct consequence of these achievements was the increasing of degradation rate of a mixture of benzotriazole and two of its derivatives (5-methyl-benzotriazole, and 5-chlorobenzotriazole). The application of chaotic flow improved the degradation of the mixture independently on the redox conditions, because all of them were occurring simultaneously. Also, the application of chaotic flow led to radial-like conditions for the full duration of the simulation period, resulting in a total reaction rate being linear with time, so that degradation is only limited by reaction kinetics. On the contrary, when chaotic flow was not applied the degradation was mostly controlled by partial mixing at very large times, controlled by the regional flow.

From another point of view, chaotic flow homogenized the system in terms of mixing and of reactive surface. This could represent that applying chaotic flow in a system would minimize the significance of heterogeneity in the transport of solutes in porous media.

To sum up, we have demonstrated that with chaotic flow we enhance the reactivity of all terminal electron acceptors increasing the total degradation rate but also the variability in the redox states. This is quite important, because it enhances and facilitates the degradation of a spectrum of Emerging Organic Compounds (here illustrated with a mixture of benzotriazoles). Applying chaotic flow is, thus, a potential intelligent methodology to eliminate a cocktail of EOCs and their metabolites by allowing the aquifer to reach many different redox states, each one of them being the most efficient one for the degradation of a given organic molecule.

Appendix A: Reaction Rates Under Radial Conditions

We consider that the degradation of benzotriazole and its derivatives is instantaneous, and controlled by the redox conditions, which themselves are controlled by the recharging water rich in organic carbon getting in contact with the aquifer water (rich in terminal electron acceptors).

After a given time, the injected water reaches a radial distance $\bar{r}$ equal to

$$\bar{r}^2 = \frac{Q}{\pi b \phi}\ t \tag{A1}$$

where ϕ is porosity and b is aquifer thickness. The distribution of concentrations of a conservative solute entering into aquifers through wells, assuming homogeneous medium and fully radial conditions, can be approximated by [e.g., *Bear*, 1972]

$$C(r,\bar{r}) = \frac{C_0}{2}\left(1-\mathrm{erf}\left(\frac{r-\bar{r}}{\sqrt{\frac{4}{3}\ \alpha\ \bar{r}}}\right)\right) \tag{A2}$$

where α is dispersivity and C_0 is the initial concentration. In this case, C stands for organic carbon. Assuming full mixing and fast degradation of the benzotriazole mixture, and its ubiquity in the system, we can consider that the concentration of the product generated from the degradation of benzotriazoles, $B(r,\bar{r})$, display a mirror image of that of organic carbon, so that

$$B(r,\bar{r}) = \frac{B_0}{2}\left(1+\mathrm{erf}\left(\frac{r-\bar{r}}{\sqrt{\frac{4}{3}\ \alpha\ \bar{r}}}\right)\right) \tag{A3}$$

The total amount of benzotriazole degraded as a function of time, $R(t)$, is thus obtained as the integral in space of $B(r,\bar{r})$

$$R(\bar{r}(t)) = \int_0^{2\pi}\int_0^{\bar{r}} B(r,\bar{r})\ r\ dr d\theta = 2\pi \int_0^{\bar{r}} B(r,\bar{r})\ r\ dr \tag{A4}$$

which is valid assuming symmetry in concentrations. The solution of this integral is

$$R(\bar{r}) = \pi\ B_0 \int_0^{\bar{r}} \left(1+\mathrm{erf}\left(\frac{r-\bar{r}}{\sqrt{\frac{4}{3}\ \alpha\ \bar{r}}}\right)\right) r\ dr = \pi\ B_0 \frac{\bar{r}^2}{4}\ f(Pe) \tag{A5}$$

where Pe is the Peclet number defined here as $Pe = \frac{\alpha}{\bar{r}}$ and the function $f(Pe)$ is

$$f(Pe) = 1 + \frac{4}{3}\sqrt{\frac{3Pe}{\pi}} - \left(\frac{2Pe}{3}+1\right)\mathrm{erf}\left(\sqrt{\frac{3}{4Pe}}\right) - \frac{2\sqrt{3Pe}}{3\sqrt{\pi}}\exp\left(-\frac{3}{4Pe}\right) \tag{A6}$$

$f(Pe)$ is a monotonously increasing function, and for large Peclet numbers ($Pe > 10$), it is approximately equal to 1, so that

$$R(\bar{r}) \approx \pi\ B_0 \frac{\bar{r}^2}{4} \tag{A7}$$

which means that

$$R(t) \approx \frac{B_0 Q}{4b\phi}\ t \tag{A8}$$

Acknowledgments
The authors thank J. Greskowiak for his support in compiling PHT3D in Linux and in High Performance Computing. Financial support was provided by the European Union, project ACWAPUR, PCIN-2015–239, WE-NEED, PCIN-2015–248; and by the Spanish government, project INDEMNE, CGL2015–69768-R (MINECO/FEDER). X.S.V. acknowledges support by the ICREA Academia Program. All data are available from the corresponding author upon request.

References

Alotaibi, M. D., B. M. Patterson, A. J. McKinley, A. Y. Reeder, A. J. Furness, and M. J. Donn (2015), Fate of benzotriazole and 5-methylbenzotriazole in recycled water recharged into an anaerobic aquifer: Column studies, *Water Res.*, *70*, 184–195.
Bagtzoglou, A., and P. Oates (2007), Chaotic advection and enhanced groundwater remediation, *J. Mater. Civil Eng.*, *19*(1), 75–83.
Banjac, Z., A. Ginebreda, M. Kuzmanovic, R. Marcé, M. Nadal, J. M. Riera, and D. Barceló (2015), Emission factor estimation of ca. 160 emerging organic microcontaminants by inverse modeling in a Mediterranean river basin (Llobregat, NE Spain), *Sci. Total Environ.*, *520*(0), 241–252.
Bauer, R. D., M. Rolle, S. Bauer, C. Eberhardt, P. Grathwohl, O. Kolditz, R. U. Meckenstock, and C. Griebler (2009), Enhanced biodegradation by hydraulic heterogeneities in petroleum hydrocarbon plumes, *J. Contam. Hydrol.*, *105*(1–2), 56–68.
Bear, J. (1972), *Dynamics of Fluids in Porous Media*, Dover, New York.
Brun, A., and P. Engesgaard (2002), Modelling of transport and biogeochemical processes in pollution plumes: Literature review and model development, *J. Hydrol.*, *256*(3–4), 211–227.
Chiogna, G., D. L. Hochstetler, A. Bellin, P. K. Kitanidis, and M. Rolle (2012), Mixing, entropy and reactive solute transport, *Geophys. Res. Lett.*, *39*, L20405, doi:10.1029/2012GL053295.
Chu, M., P. K. Kitanidis, and P. L. McCarty (2005), Modeling microbial reactions at the plume fringe subject to transverse mixing in porous media: When can the rates of microbial reaction be assumed to be instantaneous?, *Water Resour. Res.*, *41*, L20405, doi:10.1029/2004WR003495.
Cirpka, O. A., E. O. Frind, and R. Helmig (1999), Numerical simulation of biodegradation controlled by transverse mixing, *J. Contam. Hydrol.*, *40*(2), 159–182.
De Simoni, M., X. Sanchez-Vila, J. Carrera, and M. W. Saaltink (2007), A mixing ratios-based formulation for multicomponent reactive transport, *Water Resour. Res.*, *43*, W07419, doi:10.1029/2006WR005256.
Dentz, M., T. Le Borgne, A. Englert, and B. Bijeljic (2011), Mixing, spreading and reaction in heterogeneous media: A brief review, *J. Contam. Hydrol.*, *120–121*, 1–17.
Deutsch, C., and A. Journal (1992), *GSLIB: Geostatistical Software Library and User's Guide*, Oxford Univ. Press, New York.
Giorgi, F., and P. Lionello (2008), Climate change projections for the Mediterranean region, *Global Planet. Change*, *63*(2–3), 90–104.
Gramling, C. M., C. F. Harvey, and L. C. Meigs (2002), Reactive transport in porous media: A comparison of model prediction with laboratory visualization, *Environ. Sci. Technol.*, *36*(11), 2508–2514.
Greskowiak, J., H. Prommer, G. Massmann, and G. Nützmann (2006), Modeling seasonal redox dynamics and the corresponding fate of the pharmaceutical residue phenazone during artificial recharge of groundwater, *Environ. Sci. Technol.*, *40*(21), 6615–6621.
Harbaug, A. (2005), *MODFLOW-2005, The U.S. Geological Survey Modular Ground-Water Model—the Ground-Water Flow Process*, U.S. Geol. Surv. Tech. Methods 6-A16, Reston, Va.
Hughes, S. R., P. Kay, and L. E. Brown (2013), Global synthesis and critical evaluation of pharmaceutical data sets collected from river systems, *Environ. Sci. Technol.*, *47*(2), 661–677.
IPCC (2007), *Climate Change 2007: Synthesis Report*, 104 pp., IPCC, Geneva, Switzerland.
Jurado, A., E. Vàzquez-Suñé, J. Carrera, M. López de Alda, E. Pujades, and D. Barceló (2012), Emerging organic contaminants in groundwater in Spain: A review of sources, recent occurrence and fate in a European context, *Sci. Total Environ.*, *440*, 82–94.
Kitanidis, P. K. (1994), The concept of the Dilution Index, *Water Resour. Res.*, *30*(7), 2011–2026.
Lester, D. R., M. Rudman, G. Metcalfe, M. G. Trefry, A. Ord, and B. Hobbs (2010), Scalar dispersion in a periodically reoriented potential flow: Acceleration via Lagrangian chaos, *Phys. Rev. E*, *81*(4), 046319.
Liu, Y.-S., G.-G. Ying, A. Shareef, and R. S. Kookana (2013), Biodegradation of three selected benzotriazoles in aquifer materials under aerobic and anaerobic conditions, *J. Contam. Hydrol.*, *151*, 131–139.

López-Serna, R., A. Jurado, E. Vázquez-Suñé, J. Carrera, M. Petrović, and D. Barceló (2013), Occurrence of 95 pharmaceuticals and transformation products in urban groundwaters underlying the metropolis of Barcelona, Spain, *Environ. Pollut.*, *174*, 305–315.
Mayer, K. U., S. G. Benner, E. O. Frind, S. F. Thornton, and D. N. Lerner (2001), Reactive transport modeling of processes controlling the distribution and natural attenuation of phenolic compounds in a deep sandstone aquifer, *J. Contam. Hydrol.*, *53*(3–4), 341–368.
Navarro-Ortega, A., et al. (2012), Assessing and forecasting the impacts of global change on Mediterranean rivers. The SCARCE Consolider project on Iberian basins, *Environ. Sci. Pol. Res.*, *19*(4), 918–933.
Neupauer, R. M., J. D. Meiss, and D. C. Mays (2014), Chaotic advection and reaction during engineered injection and extraction in heterogeneous porous media, *Water Resour. Res.*, *50*, 1433–1447, doi:10.1002/2013WR014057.
Parkhurst, D. L., and C. A. J. Appelo (1999), User's guide to PHREEQC (version 2): A computer program for speciation, reaction-path, 1D-transport, and inverse geochemical calculations, *U.S. Geol. Surv Water Resour. Invest. Rep.*, *99–4259*, 312 p.
Pedretti, D., M. Barahona-Palomo, D. Bolster, X. Sanchez-Vila, and D. Fernàndez-Garcia (2012), A quick and inexpensive method to quantify spatially variable infiltration capacity for artificial recharge ponds using photographic images, *J. Hydrol.*, *430–431*, 118–126.
Piscopo, A. N., R. M. Neupauer, and D. C. Mays (2013), Engineered injection and extraction to enhance reaction for improved in situ remediation, *Water Resour. Res.*, *49*, 3618–3625, doi:10.1002/wrcr.20209.
Prommer, H., and P. J. Stuyfzand (2005), Identification of Temperature-Dependent Water Quality Changes during a Deep Well Injection Experiment in a Pyritic Aquifer, *Environ. Sci. Technol.*, *39*(7), 2200–2209.
Prommer, H., and V. Post (2010), *A Reactive Multicomponent Transport Model for Saturated Porous Media. User's Manual. v2.10*.
Prommer, H., D. A. Barry, and G. B. Davis (2002), Modelling of physical and reactive processes during biodegradation of a hydrocarbon plume under transient groundwater flow conditions, *J. Contam. Hydrol.*, *59*(1–2), 113–131.
Prommer, H., D. A. Barry, and C. Zheng (2003), MODFLOW/MT3DMS-based reactive multicomponent transport modeling, *Ground Water*, *41*(2), 247–257.
Prommer, H., N. Tuxen, and P. L. Bjerg (2006), Fringe-controlled natural attenuation of phenoxy acids in a landfill plume: Integration of field-scale processes by reactive transport modeling, *Environ. Sci. Technol.*, *40*(15), 4732–4738.
Rodríguez-Escales, P., and X. Sanchez-Vila (2016), Fate of sulfamethoxazole in groundwater: Conceptualizing and modeling metabolite formation under different redox conditions, *Water Res.*, *105*, 540–550.
Rodríguez-Escales, P., A. Folch, B. M. van Breukelen, G. Vidal-Gavilan, and X. Sanchez-Vila (2016), Modeling long-term enhanced in situ biodenitrification and induced heterogeneity in column experiments under different feeding strategies, *J. Hydrol.*, *538*, 127–137.
Rolle, M., T. P. Clement, R. Sethi, and A. Di Molfetta (2008), A kinetic approach for simulating redox-controlled fringe and core biodegradation processes in groundwater: Model development and application to a landfill site in Piedmont, Italy, *Hydrol. Proceses*, *22*(25), 4905–4921.
Rolle, M., C. Eberhardt, G. Chiogna, O. A. Cirpka, and P. Grathwohl (2009), Enhancement of dilution and transverse reactive mixing in porous media: Experiments and model-based interpretation, *J. Contam. Hydrol.*, *110*(3–4), 130–142.
Schirmer, M., G. C. Durrant, J. W. Molson, and E. O. Frind (2001), Influence of transient flow on contaminant biodegradation, *Ground Water*, *39*(2), 276–282.
Smale, S. (1993), on how i got started in dynamical systems, 1959–1962, in *From Topology to Computation: Proceedings of the Smalefest*, edited by M. W. Hirsch, J. E. Marsden, and M. Shub, pp. 22–26, Springer, New York.
Trefry, M. G., D. R. Lester, G. Metcalfe, A. Ord, and K. Regenauer-Lieb (2012), Toward enhanced subsurface intervention methods using chaotic advection, *J. Contam. Hydrol.*, *127*(1–4), 15–29.
Valhondo, C., J. Carrera, C. Ayora, M. Barbieri, K. Nodler, T. Licha, and M. Huerta (2014), Behavior of nine selected emerging trace organic contaminants in an artificial recharge system supplemented with a reactive barrier, *Environ. Sci. Pollut. Res. Int.*, *21*(20), 11,832–11,843.
Valhondo, C., J. Carrera, C. Ayora, I. Tubau, L. Martinez-Landa, K. Nödler, and T. Licha (2015), Characterizing redox conditions and monitoring attenuation of selected pharmaceuticals during artificial recharge through a reactive layer, *Sci. Tot. Environ.*, *512–513*, 240–250.
Werth, C. J., O. A. Cirpka, and P. Grathwohl (2006), Enhanced mixing and reaction through flow focusing in heterogeneous porous media, *Water Resour. Res.*, *42*, W12414, doi:10.1029/2005WR004511.
Ye, Y., G. Chiogna, O. A. Cirpka, P. Grathwohl, and M. Rolle (2015), Enhancement of plume dilution in two-dimensional and three-dimensional porous media by flow focusing in high-permeability inclusions, *Water Resour. Res.*, *51*, 5582–5602, doi:10.1002/2015WR016962.
Zhang, P., S. L. Devries, A. Dathe, and A. C. Bagtzoglou (2009), Enhanced mixing and plume containment in porous media under time-dependent oscillatory flow, *Environ. Sci. Technol.*, *43*(16), 6283–6288.
Zhang, W. L., Z. X. Tian, N. Zhang, and X. Q. Li (1996), Nitrate pollution of groundwater in northern China, *Agric. Ecosyst. Environ.*, *59*(3), 223–231.
Zheng, C., and P. P. Wang (1999), MT3DMS: A modular three-dimensional multispecies model for simulation of advection, dispersion and chemical reactions of contaminants in groundwater systems, in *Documentation and User's Guide, Contract Reo. SERDP-99–41*, U.S. Army Eng. Res. and Dev. Cent., Vicksburg, Miss.